

ANALYSIS OF SHALLOW WATER WAVE MEASUREMENTS RECORDED AT THE FIELD RESEARCH FACILITY

MARIOS CHRISTOU

*Shell Global Solutions International, Rijswijk, The Netherlands.
E-mail: marios.christou@shell.com*

DIRK RIJNSDORP

*TU Delft, Delft, The Netherlands and
Shell Global Solutions International, Rijswijk, The Netherlands.
E-mail: d.p.rijnsdorp@student.tudelft.nl*

KEVIN EWANS

*Sarawak Shell Bhd, Kuala Lumpur, Malaysia.
E-mail: kevin.ewans@shell.com*

1. INTRODUCTION

This paper concerns the analysis of shallow water wave measurements that have been recorded at the Field Research Facility in Duck, North Carolina, USA. This work forms parts of the NOPP ONR project. The wave measurements were recorded by four AWAC instruments in water depths of 5 m, 6 m, 8 m and 11 m. The analysis performed is threefold. First, the measured wave height statistics are compared to theoretical shallow water probability distributions. Knowledge of the wave height distribution is important for designing coastal structures (e.g. determining wave run-up, wave overtopping or the wave forces) as the wave height for a predetermined low probability of exceedence is required.

Second, the evolution of the frequency spectrum in both the cross shore location and in time is examined. This is of interest, as hindcast models provide data in deep water but this is rarely available for shallow water depths. Therefore, in the feasibility stage of designing coastal structures a simple transfer function between deep and shallow water wave spectra would be very useful, as numerical spectral models such as SWAN are computationally time consuming. Traditionally, this transfer function has been applied by the TMA spectrum (Bouws et al., 1985), however, it will be shown that this inaccurately represents the evolution of the spectrum as waves propagate from deep to shallow water.

Third, the infragravity wave energy present is compared to the Ideal Surf Beat (IDSB) numerical model. The importance of infragravity waves with respect to dune erosion during storm conditions was shown by van Thiel de Vries et al. (2008) and Roelvink et al. (2009) and Bromirski et al. (2010) found a significant impact of infragravity waves on Antarctic ice shelves. Furthermore, Naciri et al. (2004) showed the importance of incorporating infragravity waves in the calculation of moored vessel motions and Chen et al. (2004) demonstrated that infragravity waves may excite harbour seiches.

This paper continues in § 2 by describing the field measurements undertaken at the Field Research Facility. It then investigates the wave height probability distribution in § 3, evolution of the frequency spectrum in § 4 and simulation of infragravity waves in § 5. The conclusions are then drawn in § 6.

2. FIELD MEASUREMENTS

The wave data was recorded at the Field Research Facility of the US Army Corps of Engineers located in Duck, North Carolina, USA (Hanson et al., 2009). The foreshore is characterized by broad sandy beaches with a mild slope and a barred surf-zone. The tide is semi diurnal with a range of 1 m and the wave climate is characterised by locally generated wind waves and swell waves originating from the Atlantic Ocean.

There are various instruments at the facility that measure waves, winds, tides and currents. In the near-shore region two types of measurement devices are deployed, which are capable of measuring the local pressure and velocities: Nortek Aquadopp (ADOP)¹ and Nortek Acoustic Wave And Current (AWAC) meters. The velocity and pressure time series are measured with a sampling rate of 2 Hz for 34 min (4096 samples) with an interval of one hour. This sample length (2048s) is considered sufficient to accurately estimate the short-wave conditions. As infragravity waves have long periods (typical 20 s to 200 s), a sample length of 2048 s seems to be relatively short to accurately estimate the infragravity wave height. However, the influence of the sample length on the infragravity wave energy was investigated using previous measurements by a pressure array in 8 m water depth at the Field Research Facility; these measurements consisted of records with a continuous length of 2 hours and 16 minutes. It was determined that whilst the sample length influences the spectral densities, a sample length of 34 min allows for a reasonable estimation of the significant infragravity wave heights. Consequently, only the latter is considered in the present study.

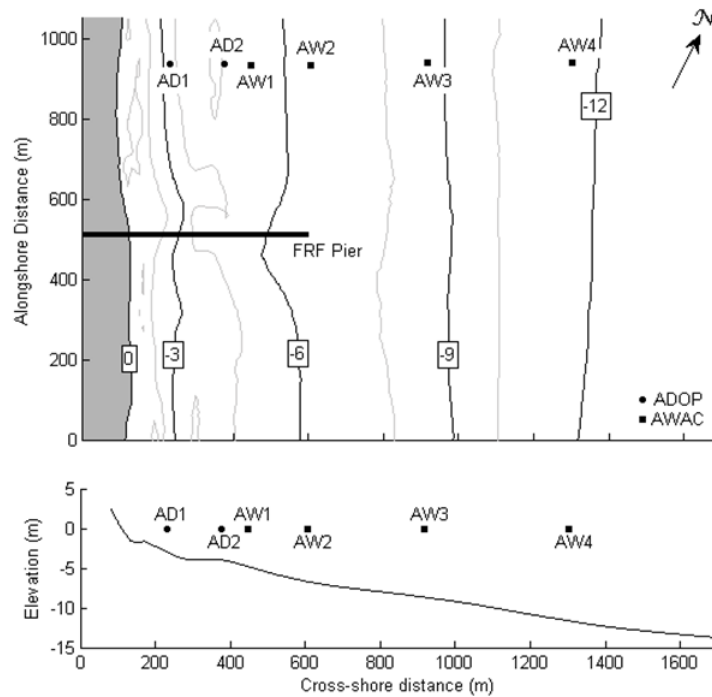


FIGURE 1. Bathymetry at the Field Research Facility. Upper panel: plan view indicating measurement instruments. Bottom panel: cross-shore profile obtained at the transect of the measurement instruments.

The time series are translated into wave height using linear wave theory and spectral densities are estimated using 13 half-overlapping Hanning windows. A window consists of 512 samples (approximately 4 min). The

¹Data only available for case E8, see Table 1

resulting spectra have a frequency resolution of 0.01 Hz and a directional resolution of 2 degrees. Figure 1 shows the instrument locations in the domain and the bathymetry, which corresponds to a survey conducted at 28th August 2010.

Table 1 present details of the five data sets available corresponding to different storms, which are identified as cases E1, E2, E3, E6 and E8. Case E2 corresponds to Hurricane Bill that occurred in 2009. For each case, measurements are available for 2 to 6 days depending on the case and the total dataset contains 1442 sea states.

Case	Date	Max. H_s [m]	Mean T_p [s]
E1	01–05 September 2010	3.2	12.3
E2	21–23 August 2009	3.3	15.1
E3	11–16 November 2009	3.0	12.0
E6	26–28 March 2009	2.9	13.6
E8	29–30 August 2010	1.7	12.7

TABLE 1. The cases analysed from data provided by the Field Research Facility.

3. WAVE HEIGHT PROBABILITY DISTRIBUTION

In this section, the measured wave height probability distribution is compared with four theoretical distributions: Rayleigh, Forristall (1978), Glukhovskiy (van Vledder, 1991) and Battjes and Groenendijk (2000). The first two are very common and typically applied for deep water, whereas the later two were specifically developed for shallow water.

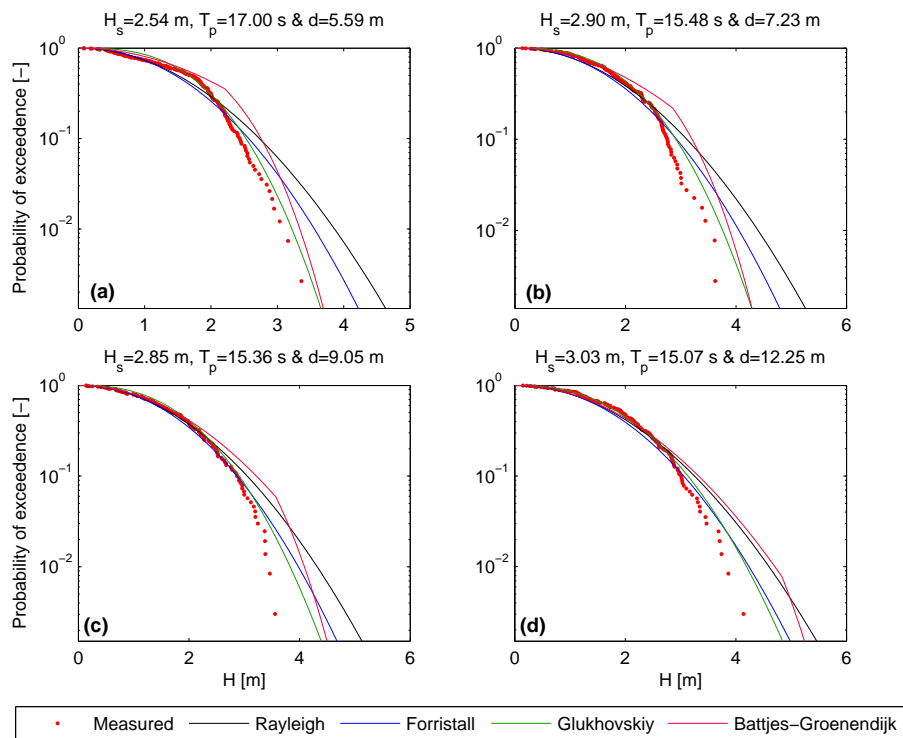


FIGURE 2. Measured and theoretical wave height probability distributions for the peak sea state during case E1 for (a) AWAC 1, (b) AWAC 2, (c) AWAC 3 and (d) AWAC 4.

Figure 2 presents a comparison of the theoretical distributions to the measured data at all AWAC instruments for the peak sea state occurring in case E1. This figure illustrates that the Glukhovskiy distribution is in best agreement with the measurements both in the body and the tail of the distribution. Focusing on the measured probability distribution, it is observed that moving from deeper to shallower water (from Figure 2(d) to (a)) there is a shift from a single (Figure 2(d)) to a double (Figure 2(a)) distribution. This later case is accommodated by the Battjes and Groenendijk (2000) distribution, which is a composite Weibull distribution. However, whilst the Battjes-Groenendijk distribution is qualitatively similar in shape to the measurements (in particular see Figures 2(a) & (b)), quantitatively they are different, as the predicted transition wave height is too high. Furthermore, despite the Battjes-Groenendijk distribution being split into two parts, the tail of the distribution is represented by a Weibull, and therefore, the wave height is unlimited. This is in contrast to the well known fact that the wave height in shallow water is limited as described by the Miche criteria (Miche, 1951). Indeed, this is a shortcoming of all of the theoretical distributions considered in the present study.

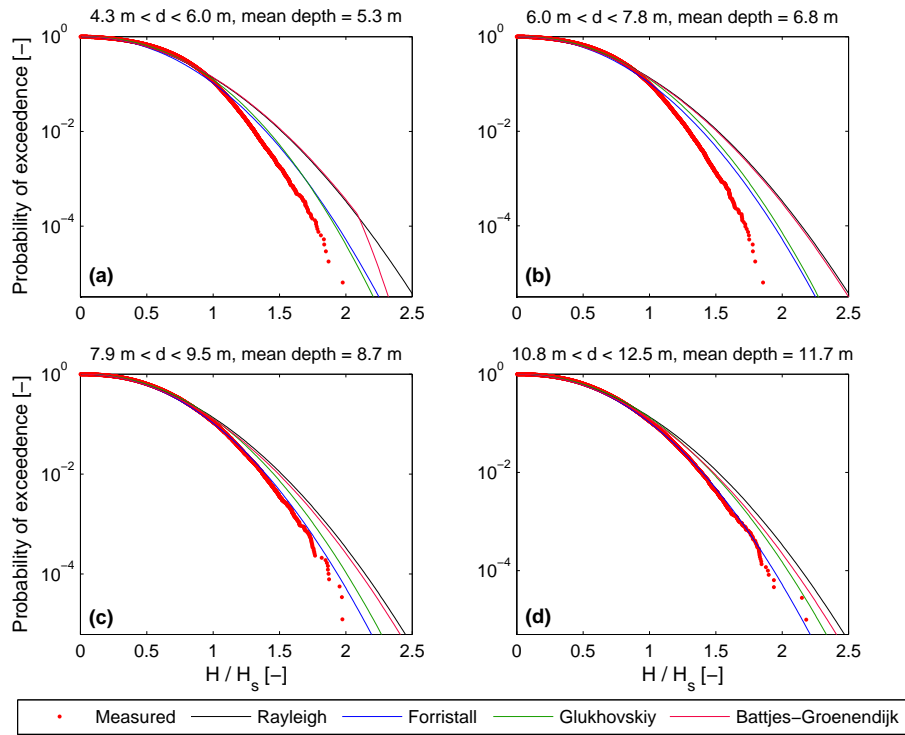


FIGURE 3. Measured and theoretical wave height probability distributions for all sea states measured by (a) AWAC 1, (b) AWAC 2, (c) AWAC 3 and (d) AWAC 4.

The discussion so far has focused on the wave height probability distribution from a single, large sea state. However, with the data from 1442 sea states, it is of interest to examine the goodness of fit of the various theoretical distributions to the larger sample size. This has been performed in two ways. First, the dependence on the water depth and significant wave height can be removed to allow visual comparisons of the measured and theoretical distributions. The water depth dependence is removed by concentrating on all the sea states at a single AWAC instrument, which limits the range of water depth for the field measurements. The mean of this range of water depths is then employed as an input to the theoretical distributions. The significant wave height dependency is removed by plotting the distribution of the wave height normalised by H_s . The result of this analysis is the 4 subplots in Figure 3. This figure demonstrates that for AWAC 4, which is in the deepest

water depth of 12.25 m, the Forristall (1978) distribution is in very good agreement with the measured data (Figure 3(d)). This is as expected, given that the Forristall (1978) distribution is an empirical fit to field data in deep water. However, the Forristall (1978) distribution appears to do very well for all AWACs, even in the mean water depth of 5.3 m (Figure 3(a)). It is however, second best to the Glukhovskiy distribution in the shallowest water depth.

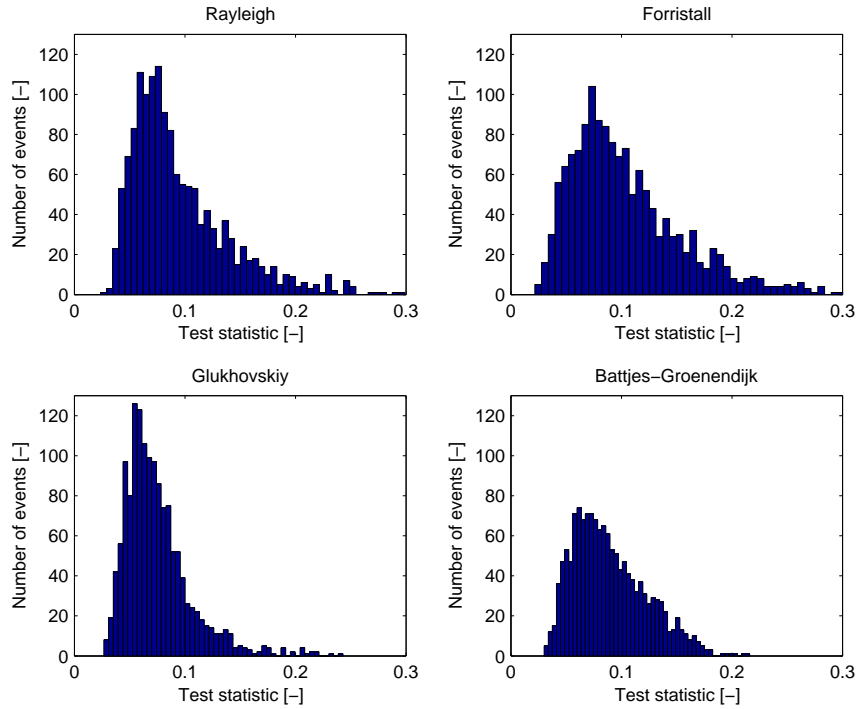


FIGURE 4. Histograms of the test statistic, k^* , for the four theoretical distributions.

Distribution	Mean k^*	Mode k^*	Median k^*	Std k^*	No. of $h = 0$
Rayleigh	0.094	0.059	0.082	0.044	1249
Forristall	0.104	0.091	0.092	0.051	1151
Glukovskiy	0.075	0.063	0.069	0.030	1390
Battjes-Gronendijk	0.089	0.059	0.084	0.033	1316

TABLE 2. Statistics from the Kolmogorov-Smirnov test, where k^* is the test statistic. The final column presents the number of sea states (out of 1442) for which the theoretical and measured distributions are the same at the 5% significance level.

Second, a statistical Kolmogorov-Smirnov (KS) test can be performed to examine the goodness of fit of the different theoretical distributions to the field measurement for each individual sea state. The null hypothesis ($h = 0$) of the KS test states that the two distributions are the same at the 5% significance level. Furthermore, the test statistic, k^* , is defined as the maximum difference between the CDFs of the two distributions. All four theoretical distributions have been compared to the field measurements and the mean, mode, median and standard deviation of the test statistic are presented in Table 2. This table also presents the number of sea

states for which the null hypothesis is correct, ie the theoretical and measured distributions are the same at the 5% significance level. Furthermore, histograms of the test statistic, k^* , are presented in Figure 4. This figure together with Table 2 demonstrate that the Glukhovskiy distribution overall compares best to the field measurements.

4. EVOLUTION OF THE FREQUENCY SPECTRUM

In this section we examine the characteristics of the spectral evolution of the frequency variance density spectra through time and space. The spectra derived from the four AWAC instruments during the three events - E1, E2, and E3 - were analysed. Examination of frequency-direction spectra at each of the locations during each of the events indicated that the predominant spectral energy was propagating cross-shore, and apart from this observation, we do not consider direction of propagation further. To examine the spatial evolution we focus on the differences between the spectra at the 5 m location by comparison with those at 11 m. By way of example, we present various representations of the observed spectral evolution for the event E1. The effects observed in the other two events are noted to be both qualitatively and quantitatively similar. The variance density spectra at the 11 m and 5 m locations, together with the gain, expressed in decibels, for E1 are plotted in the form of a spectral time history in Figure 5.

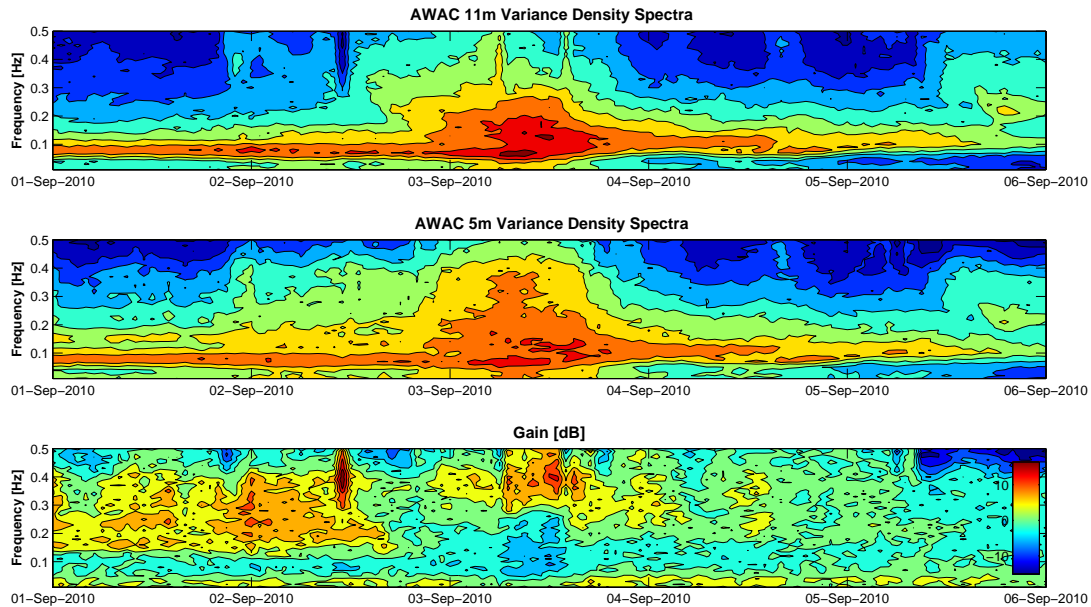


FIGURE 5. Spectra and gain during the event E1. The upper plot is the spectrogram for the 11 m AWAC, the middle plot is the spectrogram for the 5 m AWAC, and the lower plot is the ratio of the spectra of the 5 m AWAC to the 11 m AWAC expressed in dB. The colour green indicates regions in time and frequency space when the gain is approximately 0 dB.

Figure 5 shows the development of the wave field, starting during 2th September 2010 and peaking around 24 hours later. The spectra develop in unison at both the 11 m AWAC and 5 m AWAC locations, but the spectral levels are somewhat reduced at the 5 m AWAC location, reflecting attenuation from breaking and bottom dissipation, as expected with waves propagating into shallow water. The gain spectrogram in the lower plot indicates that attenuation occurs in the region of the peak frequency, and that the attenuation is greatest

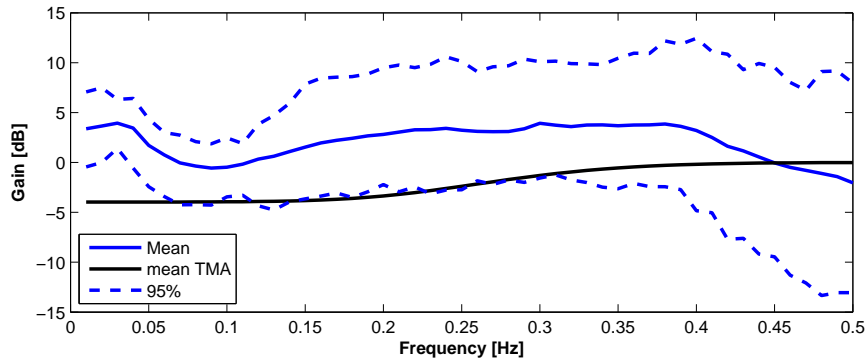


FIGURE 6. The mean gain, the 95% range, and the mean TMA spectral transfer function for the event E1.

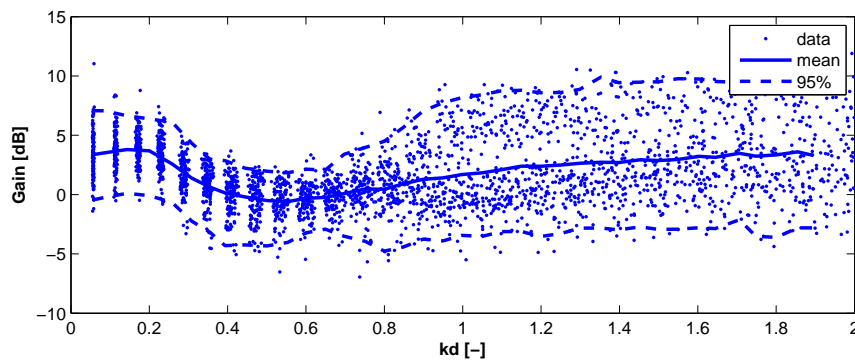


FIGURE 7. Gain against kd for all the E1 spectra. The mean (continuous line) and the 95% range (dashed lines) are also given.

when the spectral levels are at their largest. For the most part, at frequencies above and below the peak the gain is predominately positive, a likely consequence of second-order effects.

Figure 6 shows the result of considering all the spectra together through event E1. The figure gives the mean gain spectrum and curves indicating the 95% range of the gain as a function of frequency. The overall net attenuation at frequencies corresponding to the peak of the spectra is clear; though on average it is only slightly less than zero. On the other hand the overall gain at higher and lower frequencies is most notable. The average TMA spectral transfer function (Bouws et al., 1985) is also given for comparison, and while it is similar to the mean gain of the data, is approximately 4–5dB lower through most of the frequency range, and much larger at lower frequencies where infragravity waves are dominant.

The spectral frequencies were converted to the corresponding linear wave number, using the locally-measured water depths at each AWAC instrument, and the comparable spectral statistic as for Figure 6 calculated. The result is in Figure 7, which is qualitatively similar to Figure 6, but indicating that the largest attenuation is in the region of the peak frequency corresponding to a range of kd of around 0.4 to 0.5.

The indication from the data for the three events was that the attenuation is largest in the region of the peak frequency and that it increases with increasing spectral level. To demonstrate this we combined all spectra from all events and plot the gain as a function of spectral density level in Figure 8.

The blue points in Figure 8 are the data for case E1, the green points for case E2, and the red points for case E3. The plots show clearly the increase in attenuation with increasing spectral density levels over all ranges of

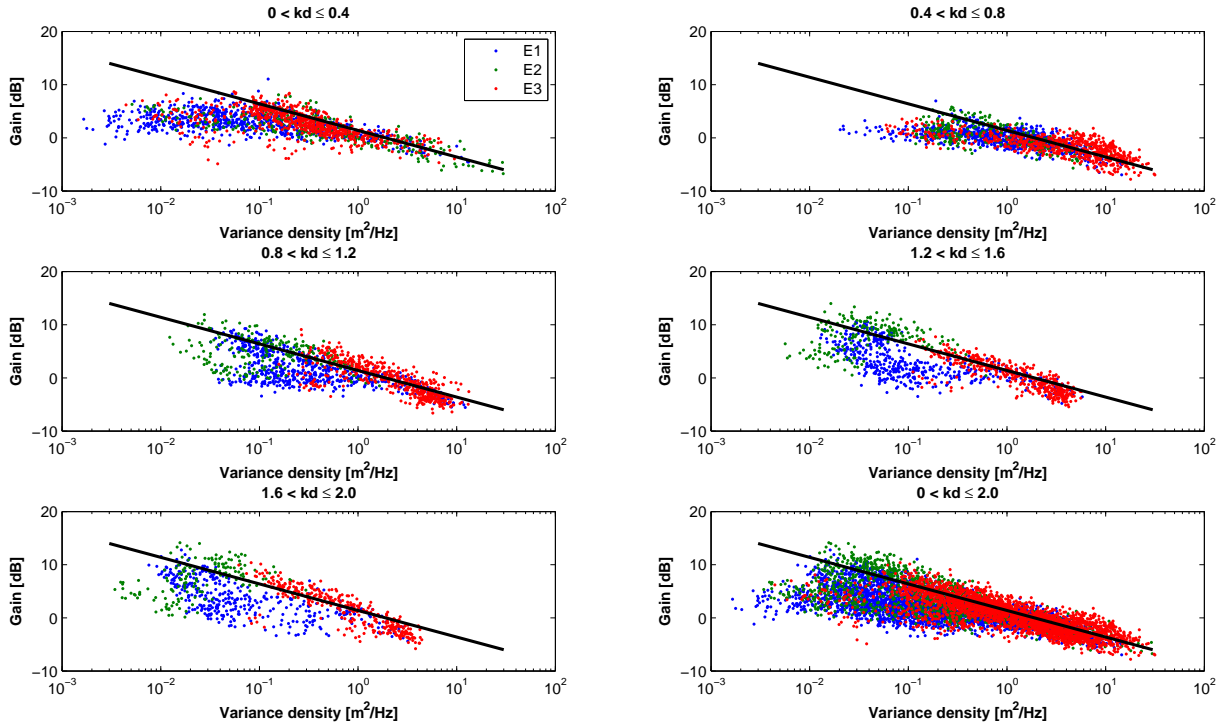


FIGURE 8. Gain versus spectral density level for the spectra from all events, stratified by kd . The straight line with a slope of -5.5 is given for comparison.

kd . The effect is most noticeable for large spectral levels, and there is good agreement for all three events at the higher spectral levels. A line with a slope of -5.5 is included, to give an indication of the rate of increase of attenuation with spectral density level. Apparently the spectral density levels must exceed some $2\text{--}3\text{ m}^2/\text{Hz}$ in order for there to be a net attenuation. Frequency components with spectral density levels lower than this generally increase from the 11 m AWAC location to the 5 m AWAC location.

5. SIMULATION OF INFRAGRAVITY WAVE ENERGY

This section concerns the simulation of infragravity wave energy at the Field Research Facility by the Ideal Surf Beat (IDSB) model. IDSB is a linear surf-beat model that describes the near-shore generation of bound infragravity waves due to directionally spread short-waves, including the near-shore propagation and the subsequent release of free infragravity waves due to reflection at the shoreline. The bathymetry is assumed to be alongshore uniform and the off-shore boundary conditions are considered alongshore periodic. Detailed information regarding the near-shore transformation of the short-waves is described by Reniers and Battjes (1997) and the infragravity wave formulation is presented by Reniers et al. (2002).

IDSB is applied to estimate the infragravity wave height at the various instruments, based on the frequency-directional spectra measured at AWAC 4, which is the most offshore location in the present study. Only cases E2, E6 and E8 were analysed for infragravity waves, as these cases consist of the highest mean peak periods (see Table 1) and will therefore generate the largest infragravity wave energy. There are several parameters that are required by IDSB, such as the wave breaking parameter, γ , that is calculated using the equation proposed by Battjes and Stive (1985)

$$\gamma = 0.5 + 0.4 \tanh(33s_0) \quad (1)$$

where s_0 is the deep water wave steepness, which is the ratio of the deep water wave height over the deep water wave length. For the simulations, the significant short-wave height and peak period as measured at AWAC 4 were used in the calculation of s_0 .

IDSB also requires the tuning of a bottom friction coefficient that not only represents physical processes due to dissipation by the sea bed, but also artificially dampens the edge waves created by the linear model, which are normally damped by nonlinear physical processes. The friction coefficient is tuned separately for each case: a representative severe and mild condition is chosen and for these two conditions the optimal friction coefficient is determined. The results showed that, for all cases, a friction coefficient of 0.009 is optimal for both the severe and mild condition. The friction coefficient is therefore set at 0.009 for all simulations, which is a slightly greater value than the friction coefficient used in previous studies at the Field Research Facility (Reniers et al., 2002, 2010) that employed a friction coefficient of 0.007.

A comparison between the IDSB simulations and the field measurements is made using the integral wave heights. The cut-off frequency that defines the upper limit of the infragravity wave frequencies and the lower limit of the short-wave frequencies is selected based on the wave spectrum. The cut-off frequency was chosen to be 0.04 Hz for case E2 and 0.03 Hz for cases E6 and E8. For all cases the upper frequency limit of the short waves is set at 0.5 Hz and the lower frequency limit of the infragravity waves is set at 0.01 Hz to disregard the mean surface elevation.

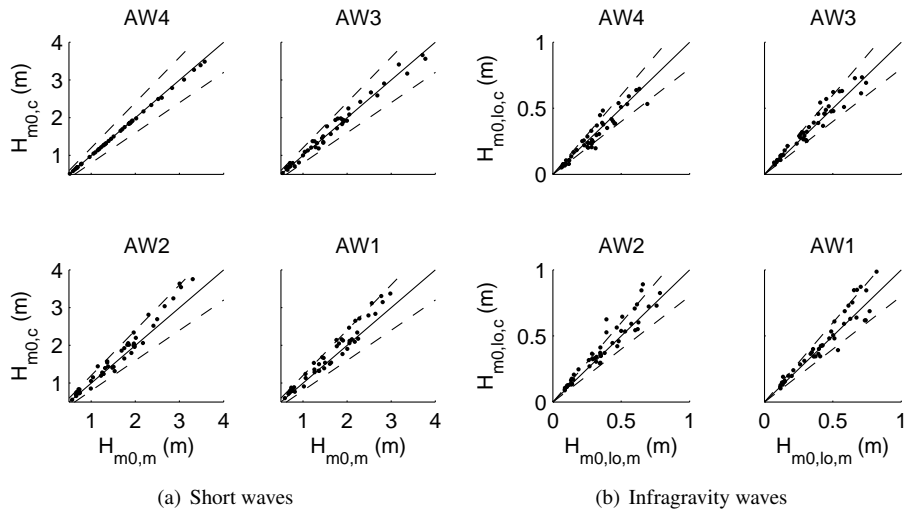


FIGURE 9. Comparisons of the significant wave height as determined from numerical simulations and field measurements for the E2 storm; the dashed lines indicate the 20% error bands.

Considering the significant short-wave height, Figures 9(a), 10(a) and 11(a) present comparisons of the numerical simulations and field measurements for cases E2, E6 and E8 respectively. These figures indicate that generally the results lie within the 20% error bands, as indicated by the dashed lines. For cases E2 and E8 the results are scattered around the line of perfect agreement, while for case E6 IDSB tends to generally over predict the short-wave height. Additionally the results indicate that for all cases IDSB tends to over predict the short-wave heights for more energetic conditions (approximately $H_{m0,m} > 1.5$ m).

Similarly, the significant infragravity wave height is presented in Figures 9(b), 10(b) and 11(b) for comparisons of the numerical simulations and field measurements for cases E2, E6 and E8 respectively. Once again, these figures show that IDSB simulations are reasonably accuracy with the majority of the results lying within

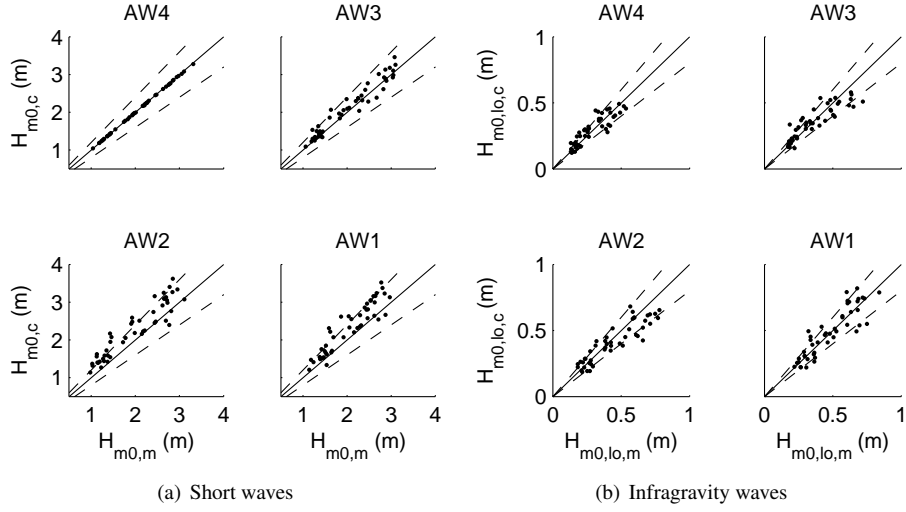


FIGURE 10. Comparisons of the significant wave height as determined from numerical simulations and field measurements for the E6 storm; the dashed lines indicate the 20% error bands.

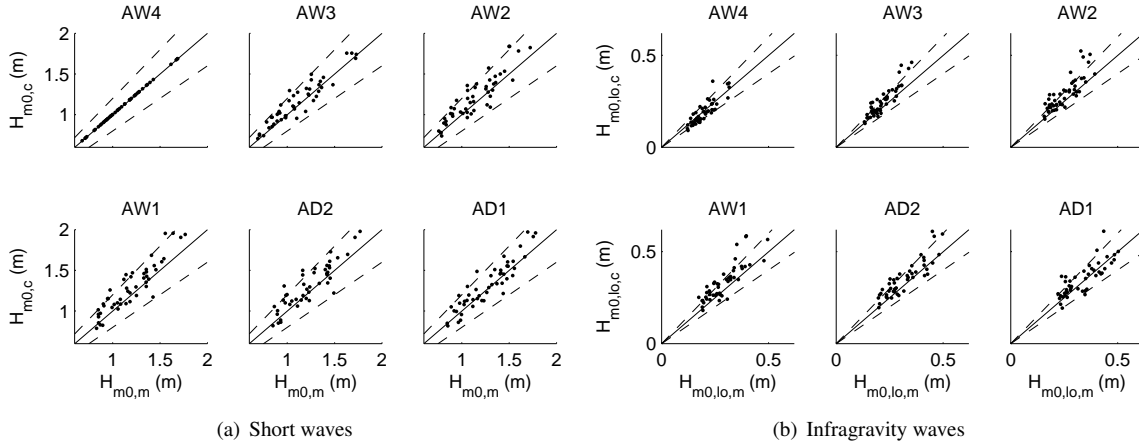


FIGURE 11. Comparisons of the significant wave height as determined from numerical simulations and field measurements for the E8 storm; the dashed lines indicate the 20% error bands.

20% of the field measurements. In general the scatter of the results increases as the instrument location moves towards the shore and the infragravity wave height is over predicted for larger measured wave heights.

In accordance with previous studies (Reniers et al., 2002, 2010), the predictive capabilities of the IDSB model are assessed with a skill level, s , expressed as

$$s = 1 - \frac{\sqrt{\langle (H_{rms,m} - H_{rms,c})^2 \rangle}}{\langle H_{rms,m}^2 \rangle} \quad (2)$$

where $H_{rms,m}$ and $H_{rms,c}$ are the measured and predicted root mean square wave heights, respectively, and $\langle \dots \rangle$ denotes averaging over all simulations. In this manner the skill is determined at every instrument for all three cases. The predictive skill gives an indication of the magnitude of the difference between the measurements and the predictions relative to the measured value. For a skill level of $s = 1$ the error is zero while for a value of $s = 0$ the error is equal to the measured value. Table 3 presents the skill level at every instrument and the overall skill for all three cases. The results show that IDSB is capable of predicting the infragravity wave conditions at a specific site with an average skill level of $s = 0.78$. The results further indicate that the skill is of similar order of magnitude at most instruments for all three cases. This level of skill is similar to that reported in previous studies (Reniers et al., 2002, 2010).

Case	AW4	AW3	AW2	AW1	AD2	AD1	Overall
E2	0.78	0.83	0.78	0.73	-	-	0.78
E6	0.78	0.75	0.74	0.81	-	-	0.77
E8	0.83	0.78	0.74	0.75	0.8	0.81	0.79

TABLE 3. Predictive skill of IDSB at the various measuring instruments and overall for all three cases.

6. CONCLUSIONS

This paper has analysed the shallow water measurements recorded at the Field Research Facility in Duck, North Carolina, USA. The analysis consisted of investigating the wave height distribution, examining the evolution of the frequency spectrum and simulating the infragravity wave energy generated at the location. By means of a Kolmogorov-Smirnov test on every sea state, it was determined that the Glukhovskiy distribution (van Vledder, 1991) provided a better fit to the measured wave height than the Rayleigh, Forristall (1978) or Battjes and Groenendijk (2000) distributions. In terms of the evolution of the frequency spectrum, it was found that the transfer function within TMA (Bouws et al., 1985) was not comparable with the field measurements, particularly at the low frequencies of the spectrum. Furthermore, it was shown that there is greater attenuation with increasing spectral density levels over all ranges of kd . Finally, the Ideal Surf Beat (IDSB) model was found to accurately predict the significant infragravity wave height with an average skill level of 78%.

ACKNOWLEDGEMENT

The authors gratefully acknowledge the funding of the Office of Naval Research as part of the NOPP project, the data provided by the US Army Corps. of Engineers from the Field Research Facility and the support of Shell Global Solutions International and TU Delft.

REFERENCES

- Battjes, J. A. and H. W. Groenendijk (2000). Wave height distributions on shallow foreshores. *Coastal Engineering* 40(3), 161 – 182.
- Battjes, J. A. and M. J. F. Stive (1985). Calibration and verification of a dissipation model for random breaking waves. *Journal of Geophysical Research* 90, 9159–9167.
- Bouws, E., G. H., W. Rosenthal, and C. L. Vincent (1985). Similarity of the wind wave spectrum in finite depth water. Part 1 - spectral form. *Journal of Geophysical Research* 90, 975–986.
- Bromirski, P. D., O. V. Sergienko, and D. R. Macayeal (2010). Transoceanic infragravity waves impacting antarctic ice shelves. *Geophysical Research Letters* 37, L02502.
- Chen, G. Y., C. C. Chien, C. H. Su, and H. M. Tseng (2004). Resonance induced by edge waves in Hua-Lien harbor. *Journal of oceanography* 60, 1035–1043.
- Forristall, G. Z. (1978). On the statistical distributions of wave heights in a storm. *Journal of Geophysical Research* 83(C5), 2353–2358.

- Hanson, J. L., H. C. Friebel, and K. K. Hathaway (2009). Coastal wave energy dissipation: Observations and STWAVE-FP performance. In *11th International Workshop on Wave Hindcasting and Forecasting & 2nd Coastal Hazards Symposium, Halifax, NS, Canada*.
- Miche, M. (1951). Le pouvoir réfléchissant des ouvrages maritimes exposés à l'action de la houle. *Annales des Ponts et Chaussées, Paris 121*, 285–319.
- Naciri, M., B. Buchner, T. Bunnik, R. Huijsmans, and J. Andrews (2004). Low frequency motions of LNG carriers moored in shallow water. In *Offshore mechanics and Arctic Engineering, Vancouver, Canada*.
- Reniers, A. and J. Battjes (1997). A laboratory study of longshore currents over barred and non-barred beaches. *Coastal Engineering 30*(1-2), 1 – 21.
- Reniers, A., M. Groenewegen, K. Ewans, S. Masterton, G. Stelling, and J. Meek (2010). Estimation of infragravity waves at intermediate water depth. *Coastal Engineering 57*(1), 52 – 61.
- Reniers, A. J. H. M., A. R. van Dongeren, J. A. Battjes, and E. B. Thornton (2002). Linear modeling of infragravity waves during Delilah. *J. Geophys. Res. 107*(C10), 3137–.
- Roelvink, D., A. Reniers, A. van Dongeren, J. van Thiel de Vries, R. McCall, and J. Lescinski (2009). Modelling storm impacts on beaches, dunes and barrier islands. *Coastal Engineering 56*, 1133–1152.
- van Thiel de Vries, J. S. M., M. R. A. van Gent, D. J. R. Walstra, and A. J. H. M. Reniers (2008). Analysis of dune erosion processes in large-scale flume experiments. *Coastal Engineering 55*, 1028–1040.
- van Vledder, G. P. (1991). Modification of the Glukhovskiy distribution. Technical report, Delft Hydraulics Report H1203.